Calculations of α/γ Phase Boundaries in Fe-C-X_1-X_2 Systems from the Central Atoms Model

T. TANAKA, H.I. AARONSON, and M. ENOMOTO

The α/γ phase boundaries in Fe-C-X_1-X_2 quaternary alloys (where X_1 = Mn and X_2 = Si, Ni, and Co, successively) are calculated from the Central Atoms model, as generalized to multicomponent systems by Foo and Lupis. The interaction parameters are evaluated from the Wagner interaction parameters in ternary iron alloys reported in the literature or estimated from the interaction parameters in binary alloys. Two equilibrium conditions, para- and orthoequilibrium, are utilized. In the Fe-C-Mn-Si system, a mixed state of equilibrium, in which orthoequilibrium is achieved with respect to C and Si while the other two substitutional elements (Fe and Mn) are assumed to be immobile (paraequilibrium), is also considered. The calculated phase boundaries are employed to evaluate the free energy change for the nucleation and the growth kinetics of proeutectoid ferrite in these alloys in companion articles.

I. INTRODUCTION

In order to analyze ferrite nucleation and growth kinetics, the volume free energy change attending nucleation and the equilibrium compositions of ferrite and austenite first must be calculated. Such thermodynamic analyses can be made using an appropriate thermodynamic model of the solid solutions involved. The Hillert–Staffansson (HS) regular solution model[1] is most widely used in the thermodynamic analysis of iron-base alloys.[2] In order to take into account deviations from random mixing, the quasi-chemical model[3] also has been used to analyze ferrite-austenite equilibria and the activity of carbon in iron-base alloys.[4] In this model, only atom pairs are considered in the evaluation of the positional entropy. The central atoms (CA) model,[5,6,7] on the other hand, considers the most probable atom configuration among all atoms in the nearest-neighbor shell of each atom. Because this is a larger atom cluster than the one used in the quasi-chemical model, the accuracy of evaluating the positional entropy and the cohesive energy of the whole system is much improved.[6] The free energy formulas of the CA model for two-sublattice (substitutional and interstitial solutes) multicomponent systems were given by Foo and Lupis.[8] Enomoto and Aaronson[9] used these formulas to calculate the ferrite(α)-austenite(γ) equilibrium phase boundaries and the free energy changes attending the proeutectoid ferrite reaction in Fe-C-X alloys.

In the first part of this article, activity expressions for quaternary Fe-C-X_1-X_2 systems are derived from the equations given by Foo and Lupis.[8] Second, using these expressions, the para- and orthoequilibrium phase boundaries in the three quaternary systems of interest in this set of articles are calculated. The three quaternary systems are Fe-C-X_1 (= Mn)-X_2 (= Si, Ni, or Co). Manganese was chosen as X_1 because it has long been known as a powerful increaser of hardenability and also a relatively tame alloying element that neither readily gives rise to a bay in the time-temperature-transformation (TTT) diagram nor produces dense arrays of carbides at austenite:ferrite boundaries. The three X_2 elements were chosen for similar reasons. Mn and Ni are well-known γ stabilizers, Si is an α stabilizer, and Co is supposed to be neutral. These systems thus yield the combination effects of $\gamma + \alpha$, $\gamma + \gamma$ and γ + neutral stabilizers in quaternary systems. It is interesting to see how these combinations affect $\gamma/(\alpha + \gamma)$ phase boundaries on the basis of the counterpart Fe-C-Mn ternary system. Paraequilibrium is a thermodynamic state in which the ratio of the number of substitutional alloying element atoms to Fe atoms is the same in ferrite as in austenite.[10] On the other hand, equilibrium with respect to all component species is achieved in the orthoequilibrium state. In a quaternary system, we can also conceive of an intermediate state in which equilibrium with respect to carbon and one substitutional element with a higher diffusivity in austenite than the second substitutional element is achieved. We denote this state as partial paraequilibrium.

In the generalization of the CA model to multicomponent systems, pairwise interaction between atoms is assumed.[8] Hence, all of the parameters necessary for the calculation can be determined from thermodynamic data in ternary systems. The same parameter values used in the calculation of Fe-C-X ternary systems[9] can be applied to the quaternary systems. Thus, the number of parameters used in the calculation of quaternary systems is considerably less in the CA than in the HS model. The only parameters that do not appear in the ternary CA calculations are the interaction parameters between X_1 and X_2 in iron. In this study, they are evaluated approximately from an expression derived by Lupis and Elliott[5] and Lupis[11] in the framework of the CA model.

T. TANAKA, formerly Graduate Student, Department of Materials Science and Engineering, Carnegie Mellon University, Pittsburgh, PA, is Chief Researcher with Steel Research Laboratories, Nippon Steel Corporation, Chiba 299-12, Japan. H.I. AARONSON, formerly R.F. Mehl Professor Emeritus at Carnegie Mellon University, is with GEO-Centers, Inc., Ft. Washington, MD, and is stationed in the Physical Metallurgy Branch, Code 6320, at the Naval Research Laboratory, Washington, DC, 20375-5343. M. ENOMOTO, Professor, is with the Department of Materials Science, Faculty of Engineering, Ibaraki University, Ibaraki 316, Japan.

Manuscript submitted September 20, 1993.

II. DERIVATION OF ACTIVITY EQUATIONS IN QUATERNARY SYSTEMS

A. *Coordination Numbers and Composition Coordinates*

In the CA model, the partition function is described in terms of probabilities associated with different configurations of the nearest-neighbor shell and the influence of these various configurations on the field acting on the substitutional or interstitial central atoms under consideration.[5,6,7]

Following the nomenclature used by Foo and Lupis,[8] an m-component solution is assumed to be composed of t substitutional solutes and m-t interstitial solutes. The configuration around a central atom J must now be characterized by the numbers i_k of nearest-neighboring substitutional solutes k ($k = 2$ to t) and the numbers j_l of the nearest-neighboring interstitial solutes l ($l = t + 1$ to m). The solvent is designated by $k = 1$. The vacancies on the interstitial sites are designated as solute $m + 1$. On the other hand, the vacancies on the substitutional sites are ignored because of their minute concentrations. Two types of coordination numbers are introduced for each substitutional or interstitial sublattice. The terms Z and z designate, respectively, the numbers of substitutional and interstitial nearest neighbors to a substitutional site, while Z' and z' designate the counterparts to an interstitial site. The lattice ratio r is defined as the ratio of the total number of interstitial sites, N_I, to the total number of substitutional sites, N_S. If N_k is the number of atoms of the kth component, then

$$N_S = \sum_{k=1}^{t} N_k, \quad N_I = \sum_{l=t+1}^{m+1} N_l \qquad [1]$$

and r is also equal to the ratio of z to Z'

$$r = \frac{N_I}{N_S} = \frac{z}{Z'} \qquad [2]$$

The coordination numbers and the value r for the body-centered cubic (bcc) and the face-centered cubic (fcc) lattices are summarized in Table I. Foo and Lupis[8] used two composition coordinates rather than the commonly used mole fractions. One is the ratio of the atoms present to the total number of sites on each sublattice for substitutional or interstitial. They are denoted as Y_i where $i = 1$, 2, 3 and C for Fe, X_1, X_2, and carbon, respectively. The other is the ratio of the number of solute atoms to the number of the solvent atoms or the vacant interstitial sites in the case of interstitial solutes. They are denoted as y_i. The two composition variables, Y_i and y_i, are written as

Table I. Coordination Numbers and r Values

	Z	z	Z'	z'	$r(= z/Z')$
Bcc	8	6	2	4	3
Fcc	12	6	6	12	1

$$Y_k = \frac{N_k}{N_S} \qquad [3a]$$

when $i = k \leq t$

$$Y_l = \frac{N_l}{N_I} \qquad [3b]$$

when $i = l > t$

$$y_k = \frac{N_k}{N_1} \qquad [4a]$$

when $i = k \leq t$

$$y_l = \frac{N_l}{N_{m+1}} \qquad [4b]$$

when $i = l > t$. The terms Y_i and y_i are related as follows to the mole fraction x_i:

$$Y_k = \frac{x_k}{1 - \sum_{l=t+1}^{m} x_l}, \qquad y_k = \frac{x_k}{1 - \sum_{i=2}^{m} x_i} \qquad [5a]$$

for $i = k \leq t$

$$Y_l = \frac{1}{r} \cdot \frac{x_l}{1 - \sum_{l=t+1}^{m} x_l},$$

$$y_l = \frac{1}{r} \cdot \frac{x_l}{1 - \sum_{l=t+1}^{m} x_l \left(1 + \frac{1}{r}\right)} \qquad [5b]$$

for $i = l > t$.

In the case of a quaternary solution of three substitutional and one interstitial species, $t = 3$, $m = 4 \equiv C$, and $m + 1 = 5 \equiv V$, where V represents vacant interstitial sites. Using Eqs. [5a] and [5b], Y_i and y_i in the quaternary Fe-C-X_1-X_2 system are described as

$$Y_1 = \frac{x_1}{1 - x_C} \qquad [6a]$$

$$Y_2 = \frac{x_2}{1 - x_C} \qquad [6b]$$

$$Y_3 = \frac{x_3}{1 - x_C} \qquad [6c]$$

$$Y_C = \frac{1}{r} \cdot \frac{x_C}{1 - x_C} \qquad [6d]$$

$$Y_V = 1 - \frac{1}{r} \cdot \frac{x_C}{1 - x_C} \qquad [6e]$$

$$y_1 = 1 \qquad [7a]$$

$$y_2 = \frac{x_2}{x_1} \qquad [7b]$$

$$y_3 = \frac{x_3}{x_1} \qquad [7c]$$

$$y_C = \frac{1}{r} \cdot \frac{x_C}{1 - x_C\left(1 + \frac{1}{r}\right)} \qquad [7d]$$

$$y_V = 1 \qquad [7e]$$

B. *Activity Equations*

In the CA model, the Gibbs free energy of mixing of the system containing t substitutional and m-t interstitial atoms is expressed as[8]

$$\begin{aligned} G^M/RT = &\sum_{k=1}^{t} n_k \ln Y_k + r\sum_{k=1}^{t} n_k \ln Y_{m+1} \\ &+ \sum_{l=t+1}^{m} n_l \ln Y_l + \sum_{J=2}^{m} n_J(Z_J\Lambda_J \\ &+ z_J\Lambda_J') - \sum_{J=1}^{m} n_J \ln P_J \\ &- \left[r\sum_{k=1}^{t} n_k - \sum_{l=t+1}^{m} n_l\right] \ln P_{m+1} \\ &- \sum_{k=1}^{m} n_k\mu_k^\circ/RT \end{aligned} \qquad [8]$$

where n_k and n_l are the number of moles of solutes k and l, and μ_k° is the chemical potential of pure component i. The terms Λ_J and Λ_J' are the Lagrangian multipliers associated with the mass balance of solute on the substitutional and institutional lattices. The term P_J is the normalization factor for the distribution probability of atoms.[8] It is expressed as the sum of the probabilities of the most probable configurations in the nearest-neighbor shell with respect to the central atom J. The activity of component i is obtained from the standard thermodynamic relationship as follows:

$$\ln a_i = \left.\frac{\partial(G^M/RT)}{\partial n_i}\right|_{n_j,P,T} \qquad [9]$$

From Eqs. [8] and [9], the activities of solvent 1, substitutional components 2 and 3, and interstitial component C are now written as

$$\begin{aligned} \ln a_1 = &\ln Y_1 + r \ln Y_V - \ln P_1 \\ &- r \ln P_V - \mu_1^\circ/RT \end{aligned} \qquad [10]$$

$$\begin{aligned} \ln a_2 = &\ln Y_2 + r \ln Y_V + Z\Lambda_2 + z\Lambda_2' \\ &- \ln P_2 - r \ln P_V - \mu_2^\circ/RT \end{aligned} \qquad [11]$$

$$\begin{aligned} \ln a_3 = &\ln Y_3 + r \ln Y_V + Z\Lambda_3 + z\Lambda_3' \\ &- \ln P_3 - r \ln P_V - \mu_3^\circ/RT \end{aligned} \qquad [12]$$

$$\begin{aligned} \ln a_C = &\ln y_C + Z'\Lambda_C + z'\Lambda_C' \\ &- \ln P_C + \ln P_V - \mu_C^\circ/RT \end{aligned} \qquad [13]$$

The Lagrangian multipliers Λ_i and Λ_i' are evaluated from the following equations:[8]

$$\Lambda_i = \ln \omega_i + \delta\varphi_{1_i}^1 \qquad [14a]$$

$$\Lambda_i' = \ln \omega_i' \qquad [14b]$$

where ω_i and ω_i' are variables, introduced[8] for mathematical convenience and related to the Lagrangian multipliers. The term $\delta\varphi_{1_i}^1$ is the difference in the energy state of the central atom Fe when one atom of the component i is present in the nearest-neighbor shell and when all the sites in the same shell are occupied by solvent Fe atoms in the substitutional lattice. The normalization factor P_J for each component is obtained through application of the general expression derived by Foo and Lupis as follows:[8]

$$\begin{aligned} P_1 = &Y_1^Z Y_V^z \exp\left[-\varphi_{0,0}^1\right](1 + y_2\omega_2 + y_3\omega_3)^Z \\ &\cdot (1 + y_C\omega_C)^z \end{aligned} \qquad [15]$$

$$\begin{aligned} P_2 = &Y_1^Z Y_V^z \exp\left[-\varphi_{0,0}^2\right]\{1 + y_2\omega_2(1 - \lambda_{2-2}) \\ &+ y_3\omega_3(1 - \lambda_{2-3})\}^Z\{1 + y_C\omega_C(1 - \lambda_{2-C})\}^z \end{aligned} \qquad [16]$$

$$\begin{aligned} P_3 = &Y_1^Z Y_V^z \exp\left[-\varphi_{0,0}^3\right]\{1 + y_2\omega_2(1 - \lambda_{2-3}) \\ &+ y_3\omega_3(1 - \lambda_{3-3})\}^Z\{1 + y_C\omega_C(1 - \lambda_{3-C})\}^z \end{aligned} \qquad [17]$$

$$\begin{aligned} P_C = &Y_1^{Z'} Y_V^{z'} \exp\left[-\varphi_{0,0}^C\right]\{1 + y_2\omega_2'(1 - \lambda_{2-C}) \\ &+ y_3\omega_3'(1 - \lambda_{3-C})\}^{Z'}\{1 + y_C\omega_C'(1 - \lambda_{C-C})\}^{z'} \end{aligned} \qquad [18]$$

$$\begin{aligned} P_V = &Y_1^{Z'} Y_V^{z'} \exp\left[-\varphi_{0,0}^V\right](1 + y_2\omega_2' + y_3\omega_3')^{Z'} \\ &\cdot (1 + y_C\omega_C')^{z'} \end{aligned} \qquad [19]$$

where λ_{J-i} is a parameter[8] of the interaction between atoms J and i. A positive value of λ_{J-i} indicates a net repulsion between these atoms, whereas a negative value demonstrates a net attraction.

Substituting Eqs. [14a], [14b], and [15] through [19] into Eqs. [10], [11], [12], and [13], the activity equations become

$$\begin{aligned} \ln a_1 = &(Z + rZ' - 1) \ln (1 + y_2 + y_3) \\ &+ \{z - r(1 - z')\} \ln (1 + y_C) \\ &- Z \ln (1 + y_2\omega_2 + y_3\omega_3) \\ &- z \ln (1 + y_C\omega_C) - r\{Z' \ln (1 + y_2\omega_2' + y_3\omega_3') \\ &+ z' \ln (1 + y_C\omega_C')\} \end{aligned} \qquad [20]$$

$$\begin{aligned} \ln a_2 = &\ln y_2 + (Z + rZ' - 1) \ln (1 + y_2 + y_3) \\ &+ \{z - r(1 - z')\} \ln (1 + y_C) \\ &- Z \ln \{1 + y_2\omega_2(1 - \lambda_{2-2}) + y_3\omega_3(1 - \lambda_{2-3})\} \\ &- z \ln \{1 + y_C\omega_C(1 - \lambda_{2-C})\} \\ &- r\{Z \ln (1 + y_2\omega_2' + y_3\omega_3') + z \ln (1 + y_C\omega_C')\} \\ &+ Z' \ln \omega_2 + z' \ln \omega_2' + Z\delta\varphi_{1_2}^1 + \varphi_{0,0}^2 - \mu_2^\circ/RT \end{aligned} \qquad [21]$$

$$\ln a_3 = \ln y_3 + (Z + rZ' - 1)\ln(1 + y_2 + y_3) + \{z - r(1 - z')\}\ln(1 + y_C) - Z\ln\{1 + y_2\omega_2(1 - \lambda_{2-3}) + y_3\omega_3(1 - \lambda_{3-3})\} - z\ln\{1 + y_C\omega_C(1 - \lambda_{3-C})\} - r\{Z\ln(1 + y_2\omega_2' + y_3\omega_3') + z'\ln(1 + y_C\omega_C')\} + Z'\ln\omega_3 + z'\ln\omega_3' + Z\delta\varphi_{1_3}^1 + \varphi_{0,0}^3 - \mu_3^\circ/RT \quad [22]$$

$$\ln a_C = \ln y_C + Z'[\ln(1 + y_2\omega_2' + y_3\omega_3') - \ln\{1 + y_2\omega_2'(1 - \lambda_{2-C}) + y_3\omega_3'(1 - \lambda_{3-C})\}] + Z'\ln\omega_C + 2z'\ln\omega_C' + Z'\delta\varphi_{1_C}^1 + \varphi_{0,0}^C - \mu_C^\circ/RT \quad [23]$$

There are additional constraints provided by the mass balance on the substitutional and interstitial lattices, *i.e.*, the conservation of the number of atoms counted for each central atom. Taylor series expansion of the mass balance equations[8] yields explicit equations for the variables ω_i and ω_i' as the polynomial form. In the quaternary 1-2-3-C systems ($m = 4$, $t = 3$), ω_i and ω_i' are given as

$$\omega_2 = 1 + \lambda_{2-2}y_2 + \lambda_{2-3}y_3 + \lambda_{2-2}(2\lambda_{2-2} - 1)y_2^2 + \lambda_{2-3}(\lambda_{2-3} + \lambda_{3-3} - 1)y_3^2 + \{\lambda_{2-2}(2\lambda_{2-3} - 1) + \lambda_{2-3}(\lambda_{3-3} + \lambda_{2-3} - 1)\}y_2y_3 + \cdots \quad [24]$$

$$\omega_3 = 1 + \lambda_{2-3}y_2 + \lambda_{3-3}y_3 + \lambda_{2-3}(\lambda_{2-2} + \lambda_{2-3} - 1)y_2^2 + \lambda_{3-3}(2\lambda_{3-3} - 1)y_3^2 + \{\lambda_{3-3}(2\lambda_{2-3} - 1) + \lambda_{2-3}(\lambda_{3-3} + \lambda_{2-3} - 1)\}y_2y_3 + \cdots \quad [25]$$

$$\omega_C = 1 + \lambda_{2-C}y_2 + \lambda_{3-C}y_3 + \lambda_{2-C}(\lambda_{2-C} - 1)y_2^2 + \lambda_{3-C}(\lambda_{3-C} - 1)y_3^2 + \{\lambda_{2-C}(\lambda_{3-C} - 1) + \lambda_{3-C}(\lambda_{2-C} - 1)\}y_2y_3 + \lambda_{2-C}^2y_2y_C + \lambda_{3-C}^2y_3y_C + \cdots \quad [26]$$

$$\omega_2' = 1 + \lambda_{2-C}y_C + \lambda_{2-C}(\lambda_{2-C} - 1)y_C^2 + \lambda_{2-C}^2y_2y_C + \lambda_{2-C}\lambda_{3-C}y_3y_C + \cdots \quad [27]$$

$$\omega_3' = 1 + \lambda_{3-C}y_C + \lambda_{3-C}(\lambda_{3-C} - 1)y_C^2 + \lambda_{2-C}\lambda_{3-C}y_2y_C + \lambda_{3-C}^2y_3y_C + \cdots \quad [28]$$

$$\omega_C' = 1 + \lambda_{C-C}y_C + \lambda_{C-C}(2\lambda_{C-C} - 1)y_C^2 + \cdots \quad [29]$$

where terms are retained up to second order, assuming that y_k and y_l are small.

Substituting Eqs. [24] through [29] into Eqs. [20] through [23], the activity equations are finally obtained as functions of y_i and the interaction parameter λ_{j-i}. From the definition of the activity coefficient at infinite dilution[11] γ_i^∞

$$\lim_{x_i \to 0}\left[\ln\frac{a_i}{x_i}\right]_{x_j \to 0} = \ln\gamma_i^\infty \quad [30]$$

and activity Eqs. [21], [22], and [23], the activity coefficients at infinite dilution are expressed as

$$\ln\gamma_2^\infty = Z\delta\varphi_{1_2}^1 + \varphi_{0,0}^2 - \mu_2^\circ/RT \quad [31]$$

$$\ln\gamma_3^\infty = Z\delta\varphi_{1_3}^1 + \varphi_{0,0}^3 - \mu_3^\circ/RT \quad [32]$$

$$\ln\gamma_C^\infty = Z'\delta\varphi_{1_C}^1 + \varphi_{0,0}^C - \mu_C^\circ/RT \quad [33]$$

Eqs. [31], [32], and [33] express the last three terms in the activity Eqs. [21], [22], and [23]. Consequently, activity Eqs. [20] through [23] are described by the composition coordinate y_i, the interaction parameter λ_{i-j}, and the activity coefficient at infinite dilution γ_i^∞.

The Wagner interaction parameter[12] is defined by the equation[11]

$$\varepsilon_i^j = \left.\frac{\partial\ln(a_i/x_i)}{\partial x_j}\right|_{x_1 \to 1} \quad [34]$$

Similarly substituting activity Eqs. [21] through [23] into Eq. [34], the relationships between the Wagner interaction coefficient ε_i^j and Foo and Lupis' interaction parameter λ_{i-j} are obtained as

$$\lambda_{i-j} = \frac{1}{2Z}\varepsilon_i^j \quad [35]$$

$$\lambda_{i-C} = \frac{1}{2Z'}\varepsilon_C^i \quad [36]$$

$$\lambda_{C-C} = \frac{r}{2Z'}\left\{\varepsilon_C^C - \left(1 + \frac{1}{r}\right)\right\} \quad [37]$$

Thus, the interaction parameter λ_{i-j} is obtained from the Wagner interaction coefficient ε_i^j.

C. *Thermodynamic Data Needed for Calculations in Fe-C-Mn-X_2 Systems*

Certain thermodynamic data are required to calculate the $\alpha + \gamma$ phase boundaries in Fe-C-Mn-X_2 systems. The values of activity coefficients and interaction parameters between solutes are needed for both the ferrite and the austenite phases. Interaction parameters are calculated from the Wagner interaction coefficients using Eqs. [35] through [37]. The value of ΔG of pure iron from austenite to ferrite is obtained from the tabulation by Orr and Chipman.[13] The other values of ΔG_i are taken from Kaufman,[14] and Kaufman and Nesor.[15] However, ΔG_{Mn} and ΔG_{Si} were modified to get a reasonable fit to the published phase diagrams.[2,16] The standard free energy difference of carbon, ΔG_C, is assumed to be zero because the standard state of carbon used in both ferrite and austenite is graphite in the calculation.[6] All of the standard free energy changes used in these computations are listed in Table II.

The activity coefficients at infinite dilution and the Wagner interaction coefficients of the alloying elements are calculated[9] from thermodynamic relationships with the equations of the excess free energy of mixing G_m^{ex}

Table II. Standard Free Energy Changes

$\Delta G_{Fe}^{bcc\rightarrow fcc}$	interpolation in a data set compiled by Orr and Chipman[13]
$\Delta G_{Mn}^{bcc\rightarrow fcc}$*	$3477.0 - 0.514\,T - 2.742 \times 10^{-3}\,T^2 + 1.6543 \times 10^{-6}\,T^3$
$\Delta G_{Si}^{bcc\rightarrow fcc}$**	$3314.0 - 2.25\,T$
$\Delta G_{Ni}^{bcc\rightarrow fcc}$	$-3932.96 - 4.1087 \times 10^{-3}\,T^2 + 0.4853 \times 10^{-5}\,T^3 - 1.41 \times 10^{-9}\,T^4$
$\Delta G_{Co}^{bcc\rightarrow fcc}$	$-6953.0 + 0.63137 \times 10^{-2}\,T^2 - 2.8037 \times 10^{-6}\,T^3$

*$\Delta G_{Mn}^{bcc\rightarrow fcc}$ was modified to fit the Fe-Mn phase diagram[16] by adding 2000 J/mole to the equation developed by Kaufman.[14]
**$\Delta G_{Si}^{bcc\rightarrow fcc}$ was developed from Uhrenius' calculated phase diagrams.[2]

compiled by Kaufman[14] and Kaufman and Nesor.[15] On carbon, the values reported by Foo and Lupis[17] are used for ln γ_C^∞ and λ_{C-C} in austenite. As for ferrite, ln γ_C^∞ is taken from Dunn and McLellan.[18] The ε_C^C value in ferrite is not available. ε_C^C in ferrite is assumed to be zero because the carbon concentration in ferrite is so small that its influence on the activity equation is negligible. The values of λ_{Mn-C} and λ_{X_2-C} are calculated from ε_C^{Mn} and $\varepsilon_C^{X_2}$ using Eq. [36]. Kirkaldy *et al.*[19] have summarized the Wagner interaction coefficients between alloying elements and carbon in austenite. Data on $\varepsilon_C^{X_2}$ are reported for some alloying elements by Foo and Lupis.[8] The interaction coefficients, λ_{X_2-C} in ferrite that are not available in the literature are assumed to be zero.

Very little data on activity coefficients and interaction parameters between the same or different species dissolved in iron have been reported. The interaction coefficients between alloying elements of different species, $\varepsilon_{Mn}^{X_2}$, that is, ε_{Mn}^{Si}, ε_{Mn}^{Ni}, or ε_{Mn}^{Co}, may be estimated from the activity coefficients in three binary systems with the equation[5]

$$\varepsilon_i^j = \ln \gamma_j^\infty|_{i-j} - \ln \gamma_i^\infty|_{1-i} - \ln \gamma_j^\infty|_{1-j} \qquad [38]$$

where 1 is the solvent iron.

Activity coefficients at infinite dilution and interaction parameters used in this calculation are summarized in Tables III and IV, respectively.

Ternary Fe-Mn-X_2 phase diagrams were calculated with the CA model to confirm the values of interaction parameter, ε_i^j, on Mn and X_2. Figures 1, 2, and 3 are calculated orthoequilibrium $\alpha + \gamma$ phase boundaries in Fe-Mn-X_2 systems, where X_2 is Si, Ni, or Co, respectively. The difference between the calculated and experimental $\gamma/(\alpha + \gamma)$ phase boundaries[20,21] is approximately 0.5 at. pct Mn at 3 at. pct Si at 700 °C in the Fe-Mn-Si alloys and is similar in the Fe-Mn-Co alloys. It is noted that Eq. [38], used to evaluate the Mn-X_2 interaction parameters, is very approximate. Considering that only a very limited amount of experimental data on the α/γ phase boundaries were reported in these systems,[20,21] a further modification of parameters was not made to force agreement with the reported phase diagrams.

III. PHASE BOUNDARY CALCULATIONS IN Fe-C-X_1-X_2 SYSTEMS

As was previously noted, two types of $\alpha + \gamma$ phase boundaries are recognized in connection with the proeutectoid ferrite reaction in Fe-C-Mn-X_2 alloys: orthoequilibrium and paraequilibrium.[22,23,24] The former represents the situation in which the partial molar free energy of each component is equal in both phases. Hence, the orthoequilibrium phase boundaries in quaternary alloys can be obtained by solving four simultaneous equations as follows:

$$G_i^\alpha = G_i^\gamma \qquad [39]$$

where i is successively 1, 2, 3 and C.

In the case of paraequilibrium,[25] the ratio of the concentration of alloying element to that of solvent Fe is constant in both phases. If this ratio is designated as θ_i

$$\theta_i = \frac{x_i^\alpha}{x_1^\alpha} = \frac{x_i^\gamma}{x_1^\gamma} = \text{const} \qquad [40]$$

where i = 2 and 3 for Mn and X_2, respectively.

Carbon atoms redistribute in a paraequilibrium situation so as to permit their partial molar free energy to become uniquely the same in austenite and ferrite:

$$G_C^\alpha = G_C^\gamma \qquad [41]$$

In the case of a quaternary system[26] where t = 3,

$$(G_1^\alpha - G_1^\gamma) + \theta_2(G_2^\alpha - G_2^\gamma) + \theta_3(G_3^\alpha - G_3^\gamma) = 0 \qquad [42]$$

and

$$\theta_2 = \frac{x_2^\alpha}{x_1^\alpha} = \frac{x_2^\gamma}{x_1^\gamma}, \qquad \theta_3 = \frac{x_3^\alpha}{x_1^\alpha} = \frac{x_3^\gamma}{x_1^\gamma} \qquad [43]$$

Table III. Activity Coefficients at Infinite Dilution

	Ferrite	Austenite
ln γ_{Mn}^∞	$(4100 + 4.686T)/RT$	$(-18{,}870 + 16.987T)/RT$
ln γ_{Si}^∞	$(-129{,}704 + 7.95T)/RT$	$(-136{,}817 + 7.95T)/RT$
ln γ_{Ni}^∞	$(1339 + 1.3275 \times 10^{-3}\,T^2 - 1.587 \times 10^{-6} \times T^3)/RT$	$(2092 - 3.8314 \times 10^{-3}\,T^2 + 1.6338 \times 10^{-6} \times T^3)/RT$
ln γ_{Co}^∞	$(-36{,}949 + 5.00 \times 10^{-2}\,T^2 - 2.170 \times 10^{-5} \times T^3)/RT$	$(-2322 + 2.084 \times 10^{-3}\,T^2 - 4.299 \times 10^{-7} \times T^3)/RT$
ln γ_C^∞	$-5.191 + 12{,}431/T$	$-2.1 + 5300/T$
ln $\gamma_{Si}^\infty\|_{Mn\text{-}Si}$	$(-92{,}885 - 23.012\,T)/RT$	$(-104{,}184 - 23.012\,T)/RT$
ln $\gamma_{Ni}^\infty\|_{Mn\text{-}Ni}$	$(45{,}606 + 3.64\,T)/RT$	$(51{,}882 + 10.878\,T)/RT$
ln $\gamma_{Co}^\infty\|_{Mn\text{-}Si}$	$-26{,}150/RT$	$-23{,}849/RT$

Table IV. Interaction Parameters

	Ferrite	Austenite
$\lambda_{Mn\text{-}C}$	—	$0.155 - 650/T$
$\lambda_{Si\text{-}C}$	$3.7 - 3750/T$	$0.403 + 614/T$
$\lambda_{Ni\text{-}C}$	—	$-0.183 + 633/T$
$\lambda_{Co\text{-}C}$	—	$233/T$
$\lambda_{C\text{-}C}$	—	$1 - \exp[-0.1 - 290/T]$
$\lambda_{Mn\text{-}Mn}$	$(-376.5 - 0.983\,T)/RT$	$(1572.5 - 1.416\,T)/RT$
$\lambda_{Si\text{-}Si}$	$(-4707 + 15.12\,T)/RT$	$(-2545.25 + 10.08\,T)/RT$
$\lambda_{Ni\text{-}Ni}$	$(-2369 + 4.095 \times 10^{-3}\,T^2 - 1.252 \times 10^{-6}\,T^3)/RT$	$(-3255 + 2.672 \times 10^{-3}\,T^2 - 1.139 \times 10^{-6}\,T^3)/RT$
$\lambda_{Co\text{-}Co}$	$(4251 - 7.044 \times 10^{-3}\,T + 3.357 \times 10^{-6}\,T/^2)/RT$	$(305 + 1.304 \times 10^{-4}\,T - 2.685 \times 10^{-8}\,T/^2)/RT$
$\lambda_{Mn\text{-}Si}$	$(2045 - 2.228\,T)/RT$	$(2146 - 1.999\,T)/RT$
$\lambda_{Mn\text{-}Ni}$	$(2510 - 6.538 \times 10^{-2}\,T^2 + 9.919 \times 10^{-8}\,T^3)/RT$	$(2861 - 2.545 \times 10^{-1}\,T + 1.596 \times 10^{-}\,T^2)/RT$
$\lambda_{Mn\text{-}Co}$	$(419 - 2.929 \times 10^{-1}\,T - 8.297 \times 10^{-5}\,T^2 + 9.919 \times 10^{-8}\,T^3)/RT$	$(-111 - 7.078 \times 10^{-1}\,T - 8.683 \times 10^{-5}\,T^2 + 1.179 \times 10^{-8}\,T^3)/RT$

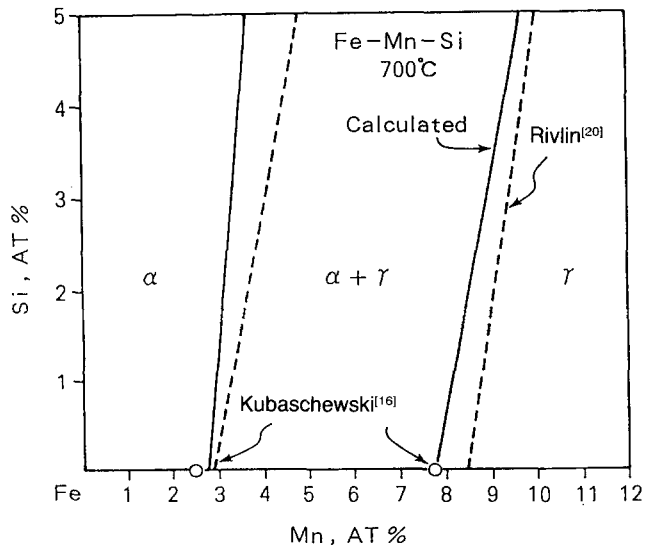

Fig. 1—Calculated phase boundaries of Fe-rich region in Fe-Mn-Si system at 700 °C.

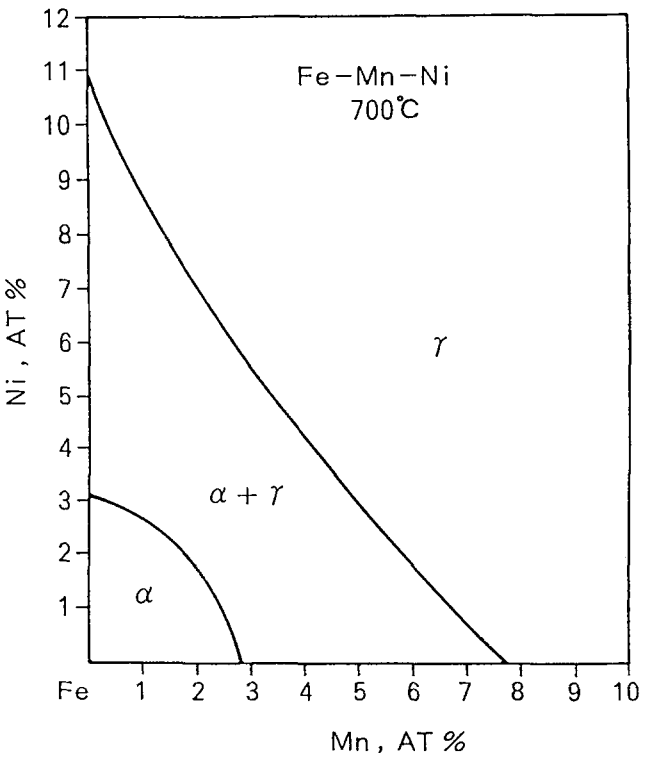

Fig. 2—Calculated phase boundaries of Fe-rich region in Fe-Mn-Ni system at 700 °C.

In Fe-C-Mn-Si system, the diffusivity of Si is considerably higher than that of Mn.[27] Accordingly, we can postulate that equilibrium is achieved with respect to both Si and C, but no partition of Mn takes place during formation of ferrite. In this case, only x_{Mn}/x_{Fe} is maintained constant and is the same in ferrite and in austenite. Such a state, here termed partial paraequilibrium, can be described as

$$G_C^\alpha = G_C^\gamma \quad [44]$$

$$G_{Si}^\alpha = G_{Si}^\gamma \quad [45]$$

$$(G_1^\alpha - G_1^\gamma) + \theta_2(G_2^\alpha - G_2^\gamma) = 0 \quad [46]$$

where 1 is Fe and 2 is Mn.

IV. RESULTS AND DISCUSSION

Figures 4, 5, and 6 show calculated orthoequilibrium phase boundaries for the $\alpha + \gamma$ region at 700 °C in three-dimensional perspective for the Fe-rich corner of the Fe-C-Mn-Si, Fe-C-Mn-Ni, and Fe-C-Mn-Co systems, respectively. Figures 7, 8, and 9 show isoconcentration sections of X_2 through orthoequilibrium phase boundaries illustrated in Figures 4, 5, and 6. As the Si or Co concentration increases, the $\alpha + \gamma$ region expands. On the other hand, as the Ni concentration increases, the $\alpha + \gamma$ region shrinks. Figure 10 shows the effects of X_2 on the orthoequilibrium $\gamma/(\alpha + \gamma)$ boundary in the Fe-C-Mn-X_2 system. Isoconcentration sections through paraequilibrium phase boundaries are shown in Figures 11, 12, and 13. Figure 14 shows the effects of X_2 alloying element on the $\gamma/(\alpha + \gamma)$ paraequilibrium phase boundary in the Fe-C-Mn-X_2 system. Figure 15 shows calculated paraequilibrium $\gamma/(\alpha + \gamma)$ boundaries at $x_{Mn}/x_{Fe} = x_{x_2}/x_{Fe} = 0.03$. Figure 16 shows sections

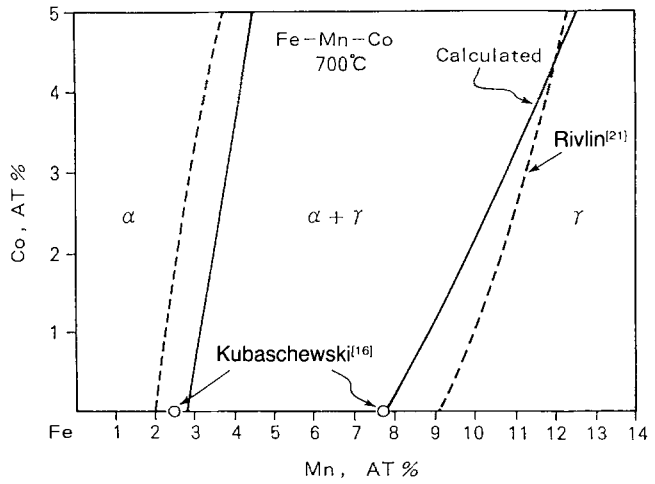

Fig. 3—Calculated phase boundaries of Fe-rich region in Fe-Mn-Co system at 700 °C.

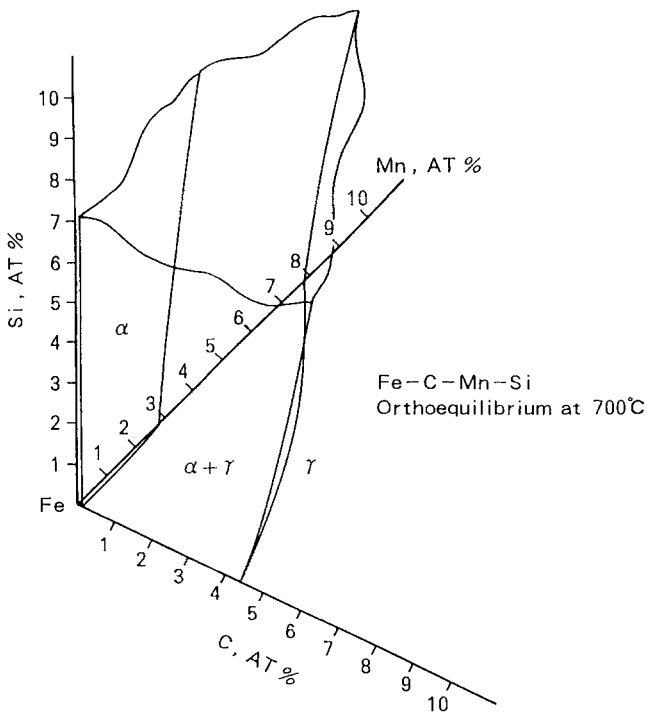

Fig. 4—Calculated orthoequilibrium phase boundaries of Fe-rich region in Fe-C-Mn-Si system at 700 °C.

of paraequilibrium, partial paraequilibrium, and orthoequilibrium $\gamma/(\alpha + \gamma)$ phase boundaries in the Fe-C-Mn-Si systems when $X_{Mn}/X_{Fe} = 0.03$. The Si component is supposed to reach equilibrium at $\alpha:\gamma$ boundaries in the partial paraequilibrium state of the Fe-C-Mn-Si system. As expected, the phase boundaries of partial paraequilibrium lie outside of the paraequilibrium phase boundaries and inside of the orthoequilibrium boundaries. Generally, the two-phase region of paraequilibrium is smaller than the orthoequilibrium phase boundaries.[23] This rule holds true with respect to partial paraequilibrium phase boundaries, as well.

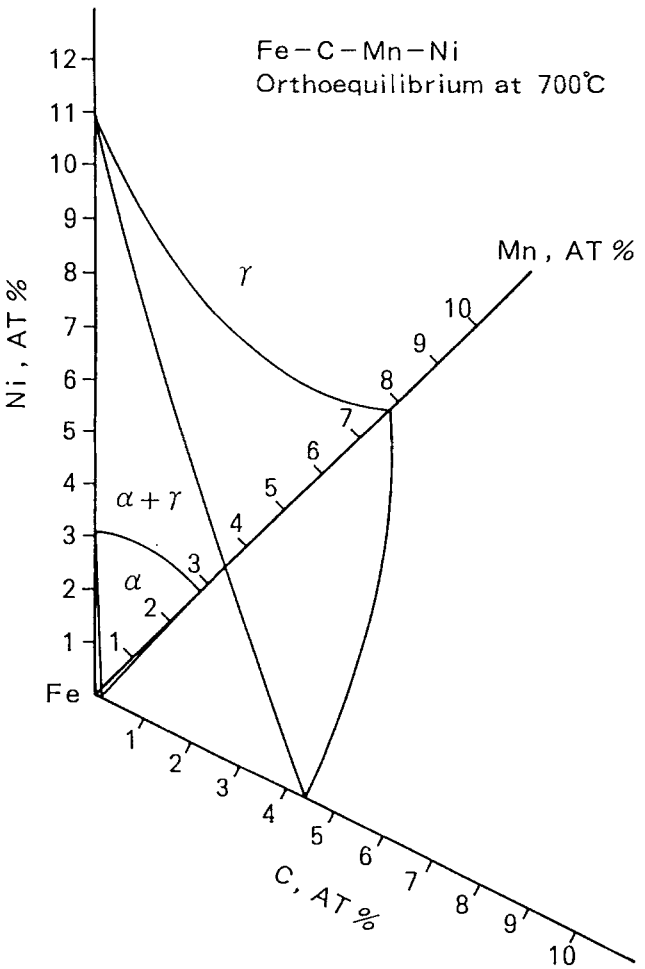

Fig. 5—Calculated orthoequilibrium phase boundaries of Fe-rich region in Fe-C-Mn-Ni system at 700 °C.

Experimental data on phase boundaries are rarely reported in quaternary Fe-base alloys. For the counterpart ternary alloys, Enomoto and Aaronson[9] found that the CA model gives generally good agreement with available experimental phase boundaries. Hence, the error associated with quaternary alloys may come from the values of the X_1 and X_2 interaction term. In Figures 1 and 3, calculated Mn compositions on $\gamma/(\alpha + \gamma)$ phase boundaries are seen to be about 0.5 at. pct smaller at 3 at. pct Si and at 3 at. pct Co at 700 °C than the experimental phase boundaries in Fe-Mn-Si and Fe-Mn-Co alloys, respectively, and thus similar displacements might be anticipated in Fe-C-Mn-Si and Fe-C-Mn-Co alloys. This error will have some effect on the volume free energy change for nucleation and the interface compositions in orthoequilibrium. In paraequilibrium, such disagreements may exert negligible effects because the Mn-X_2 interaction does not affect carbon activity significantly.

V. SUMMARY

Calculations of ferrite/austenite orthoequilibrium, partial paraequilibrium, and full paraequilibrium phase

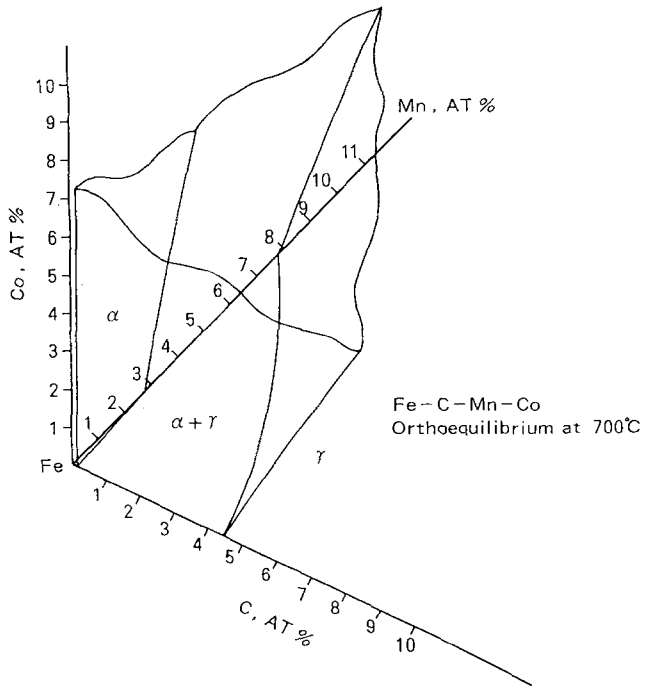

Fig. 6—Calculated orthoequilibrium phase boundaries of Fe-rich region in Fe-C-Mn-Co system at 700 °C.

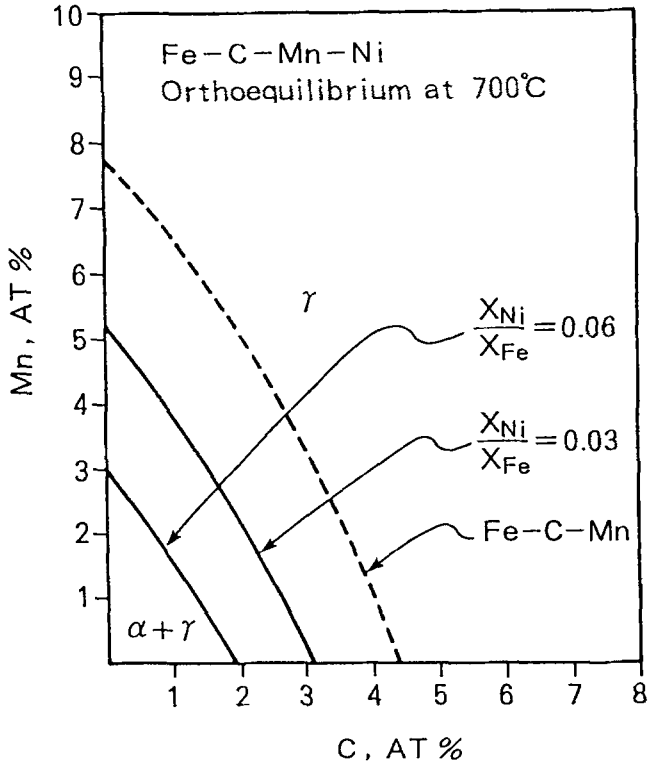

Fig. 8—Effect of Ni concentration on $\gamma/(\alpha + \gamma)$ orthoequilibrium phase boundary in Fe-C-Mn-Ni system at 700 °C.

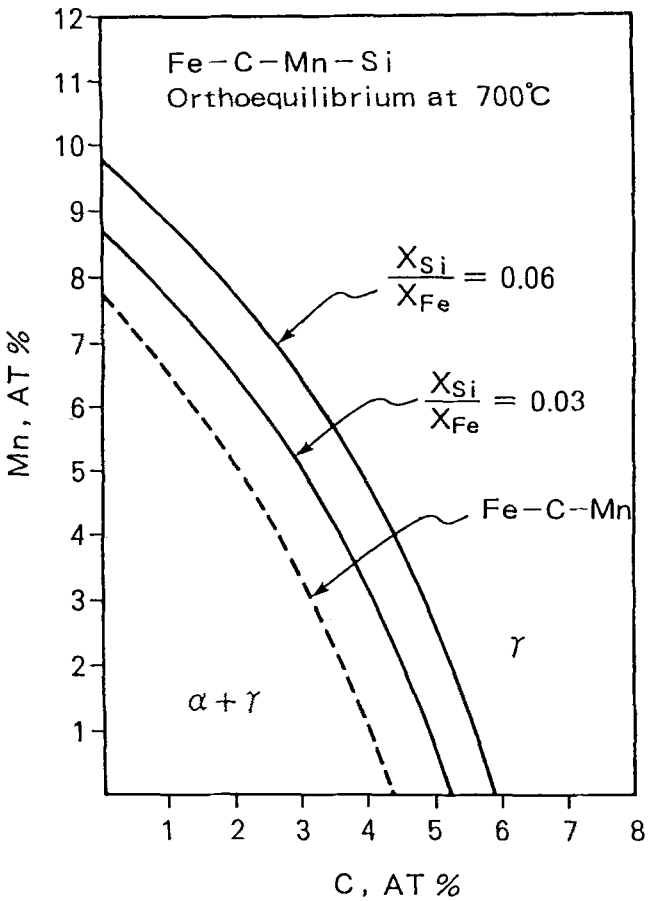

Fig. 7—Effect of Si concentration on $\gamma/(\alpha + \gamma)$ orthoequilibrium phase boundary in Fe-C-Mn-Si system at 700 °C.

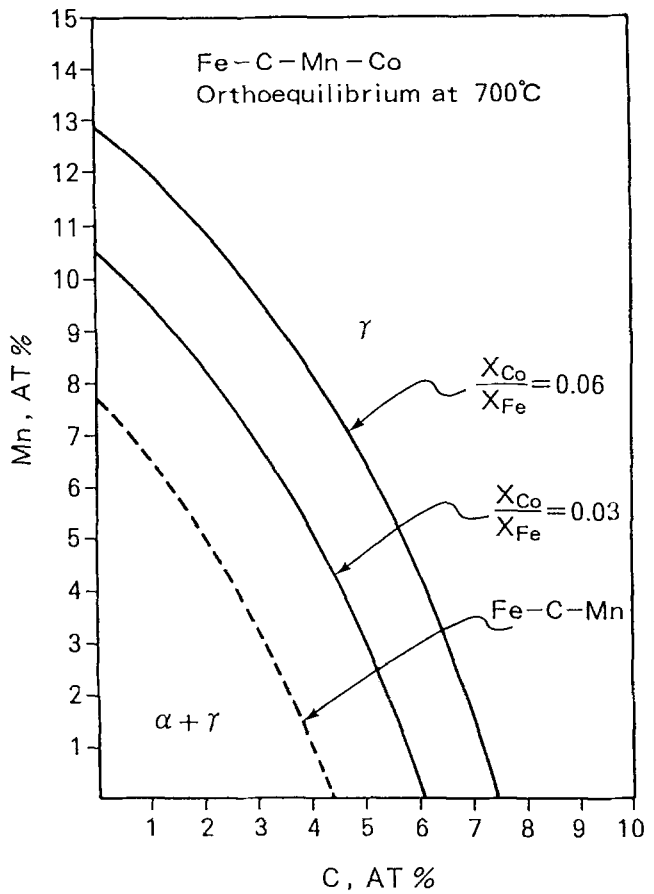

Fig. 9—Effect of Co concentration on $\gamma/(\alpha + \gamma)$ orthoequilibrium phase boundary in Fe-C-Mn-Co system at 700 °C.

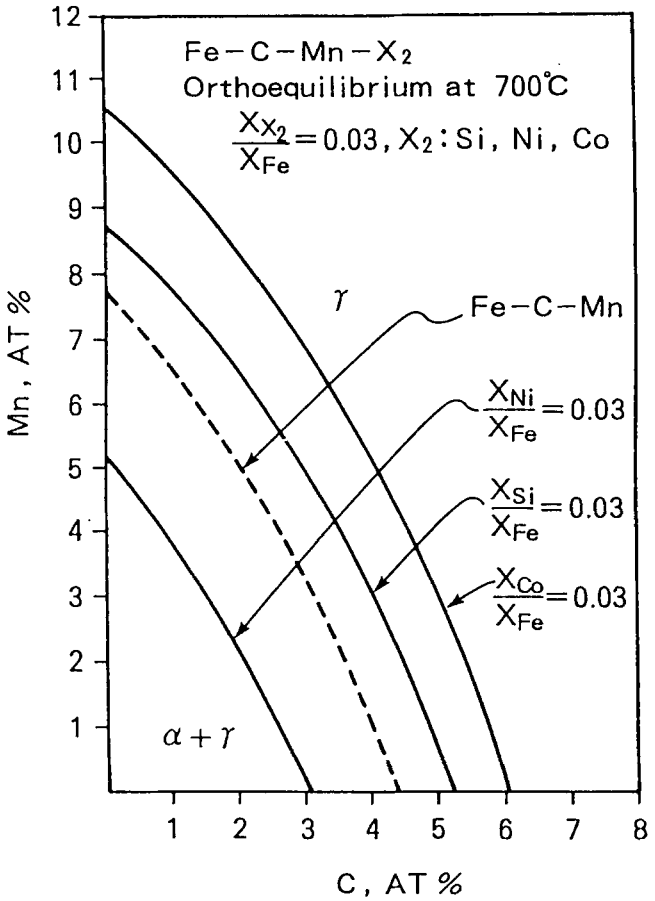

Fig. 10—Effect of X_2 alloying elements on $\gamma/(\alpha + \gamma)$ orthoequilibrium boundary in Fe-C-Mn-X_2 system at 700 °C.

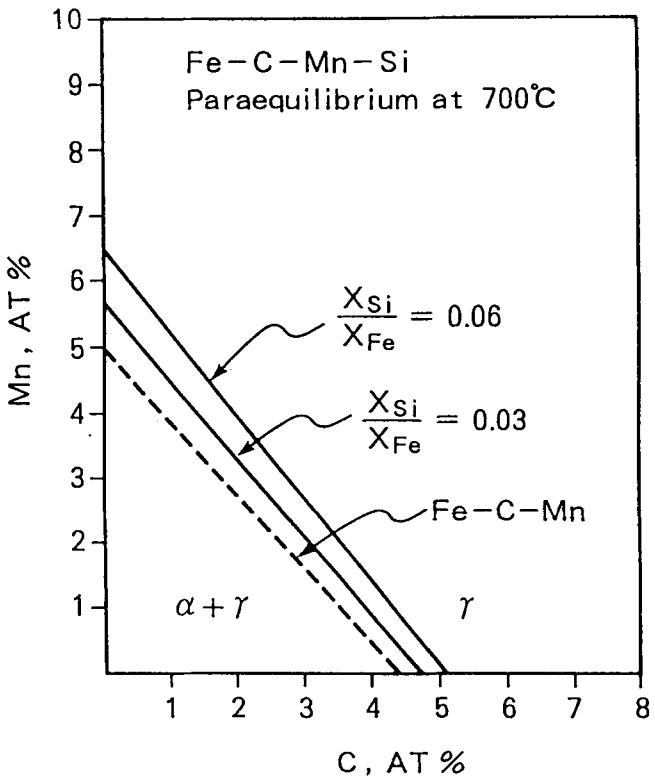

Fig. 11—Effect of Si concentration on $\gamma/(\alpha + \gamma)$ paraequilibrium boundary in Fe-C-Mn-Si system at 700 °C.

boundaries by means of the CA model,[5,6,7] previously conducted on ternary alloys,[9] have been extended to Fe-C-X_1-X_2 systems, in which X_1 is Mn and X_2 is successively Si, Ni, or Co. Activity equations in quaternary systems were first derived from general activity equations proposed by Foo and Lupis.[8] The only additional thermodynamic parameters needed to extend the calculations from ternary to quaternary systems are the interaction parameter between X_1 and X_2 elements dissolved in iron.

The combination effects of Mn + X_2(Si, Ni, or Co) have been demonstrated on $\gamma/(\alpha + \gamma)$ phase boundaries to the one of the counterpart Fe-C-Mn ternary alloy. Silicon raised the $\gamma/(\alpha + \gamma)$ phase boundary, whereas Ni depressed it, as expected. Cobalt is revealed to raise the phase boundary more than Si according to the calculations, although Co has seemed neutral.

The present calculation can be readily extended to higher order systems. As long as pairwise interaction is assumed, the number of thermodynamic parameters needed for the calculations is only moderately increased. All are evaluated from the data on activities or phase boundaries in Fe-C-X and Fe-X_1-X_2 ternary systems.

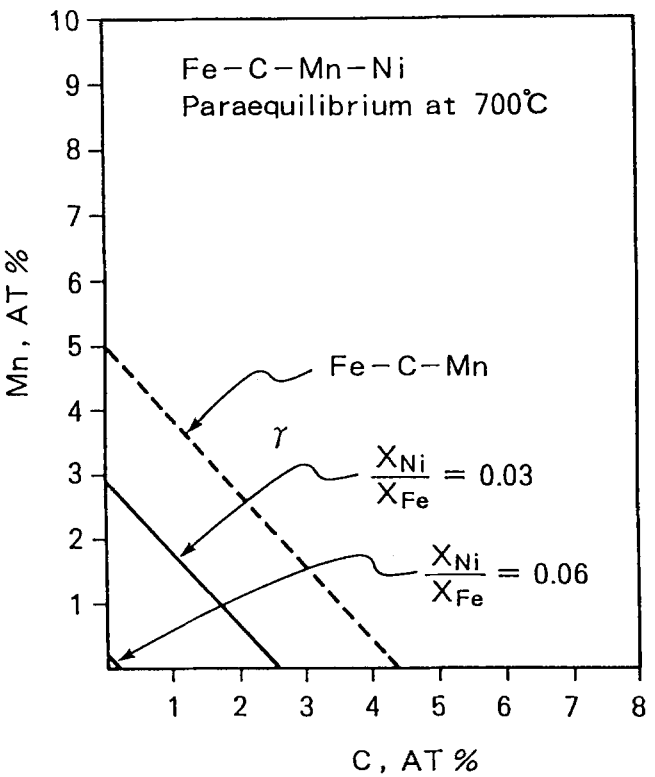

Fig. 12—Effect of Ni concentration on $\gamma/(\alpha + \gamma)$ paraequilibrium boundary in Fe-C-Mn-Ni system at 700 °C.

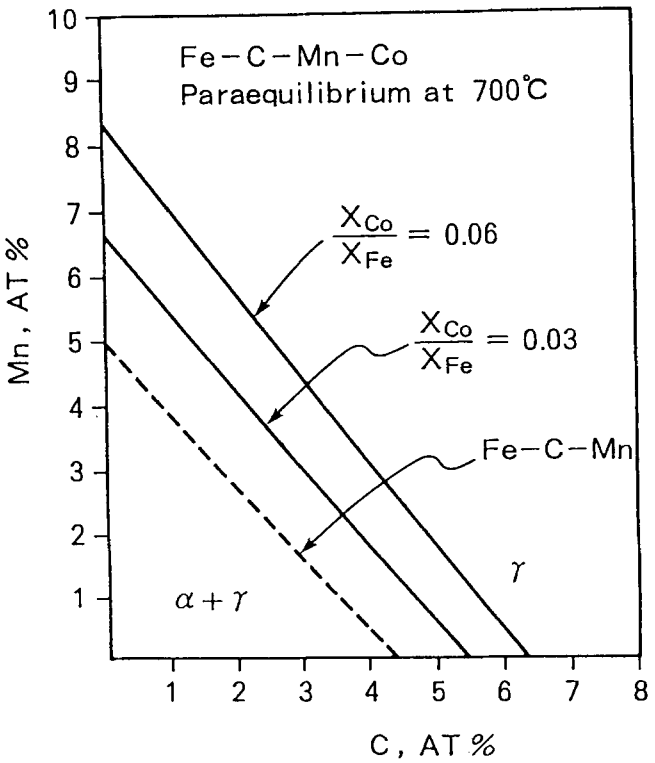

Fig. 13—Effect of Co concentration on $\gamma/(\alpha + \gamma)$ paraequilibrium boundary in Fe-C-Mn-Co system at 700 °C.

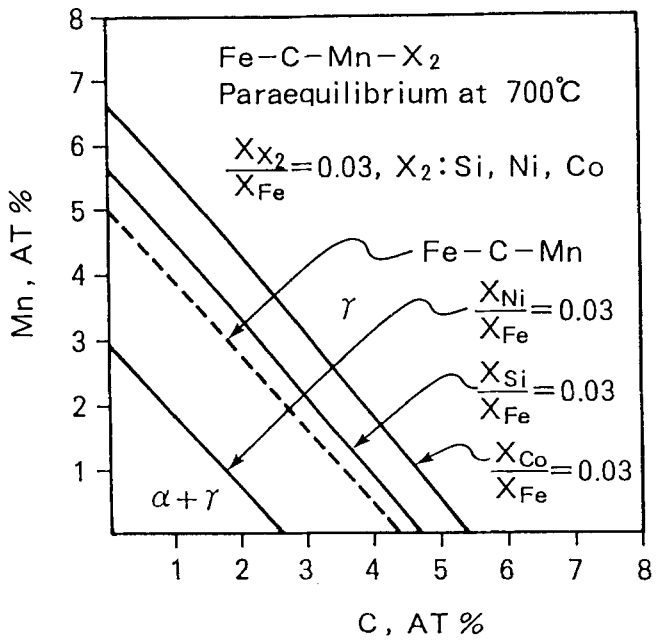

Fig. 14—Effect of X_2 alloying element on $\gamma/(\alpha + \gamma)$ paraequilibrium boundary in Fe-C-Mn-X_2 system at 700 °C.

ACKNOWLEDGMENTS

The authors thank the U.S. Army Research Office for sponsoring this investigation during its initial stages and the Nippon Steel Corporation for supporting TT and the National Research Institute of Metals for funding the contributions of ME throughout this research program.

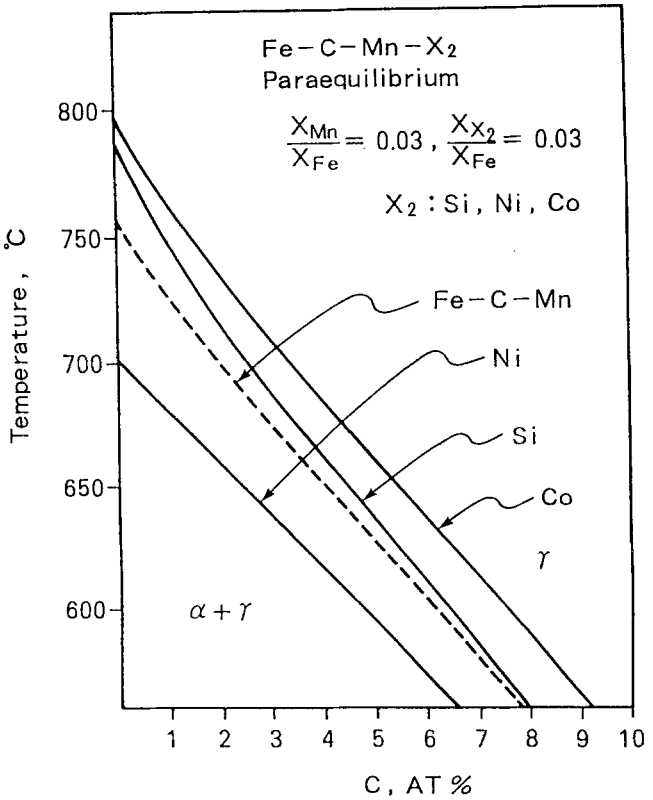

Fig. 15—Paraequilibrium $\gamma/(\alpha + \gamma)$ phase boundaries in Fe-C-Mn-X_2 alloys at $X_{Mn}/X_{Fe} = X_{X_2}/X_{Fe} = 0.03$.

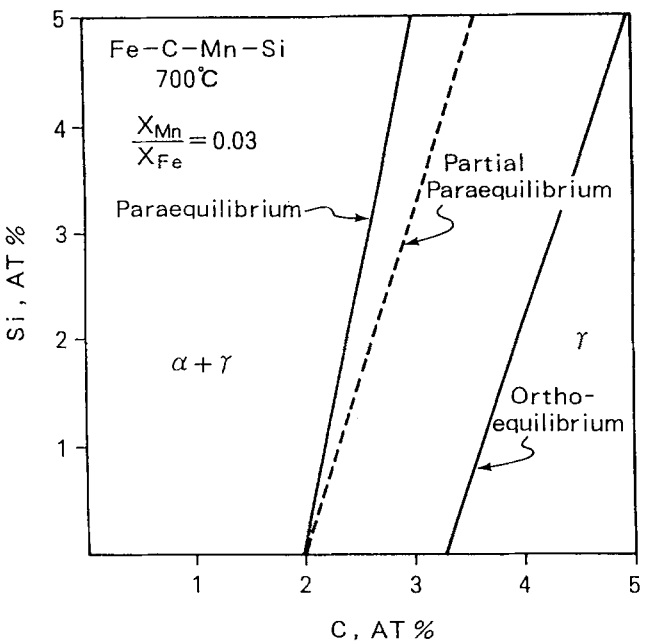

Fig. 16—Paraequilibrium, partial paraequilibrium, and ortho-equilibrium $\gamma/(\alpha + \gamma)$ phase boundaries in the Fe-C-Mn-Si system at 700 °C.

REFERENCES

1. M. Hillert and L.I. Staffansson: *Acta Chem. Scand.*, 1970, vol. 24, p. 3618.
2. B. Uhrenius: *Hardenability Concepts with Applications to Steel*, TMS-AIME, Warrendale, PA, 1978, p. 28.
3. R.B. McLellan and W.W. Dunn: *J. Phys. Chem. Solids*, 1969, vol. 30, p. 2631.
4. G.J. Shiflet, J.R. Bradley, and H.I. Aaronson: *Metall. Trans. A*, 1978, vol. 9A, pp. 999-1008.
5. C.H.P. Lupis and J.F. Elliott: *Acta Metall.*, 1967, vol. 15, p. 265.
6. C.H.P. Lupis: *Chemical Thermodynamics of Materials*, North-Holland, New York, NY, 1983, p. 452.
7. J.-C. Mathieu, F. Durand, and E. Bonnier: *J. Chim. Phys.*, 1965, vols. 11–12, p. 1289.
8. E-H. Foo and C.H.P. Lupis: *Acta Metall.*, 1973, vol. 21, p. 1409.
9. M. Enomoto and H.I. Aaronson: *CALPHAD*, 1985, vol. 9, p. 43.
10. M. Hillert: *Jernkontorets Ann.*, 1952, vol. 136, p. 25.
11. C.H.P. Lupis and J.F. Elliott: *Acta Metall.*, 1966, vol. 14, p. 529.
12. C. Wagner: *Thermodynamics of Alloys*, Addison-Wesley, Reading, MA, 1952, p. 51.
13. R.L. Orr and J. Chipman: *Trans. AIME*, 1967, vol. 239, p. 630.
14. L. Kaufman: *CALPHAD*, 1977, vol. 1, pp. 28 and 37; L. Kaufman: *CALPHAD*, 1978, vol. 2, pp. 118, 125, 128, and 130; L. Kaufman: *CALPHAD*, 1979, vol. 3, p. 57.
15. L. Kaufman and H. Nesor: *CALPHAD*, 1978, vol. 2, p. 60.
16. O. Kubaschewski: *IRON-Binary Phase Diagram*, Springer-Verlag, New York, NY, 1982, p. 62.
17. E.-H. Foo and C.H.P. Lupis: *Proc. Int. Conf. on the Science and Technology of Iron and Steel*, Tokyo, 1970, suppl. to *Trans. Iron Steel Inst. Jpn*, 1971, vol. 11, p. 404.
18. W.W. Dunn and R.B. McLellan: *Metall. Trans.*, 1971, vol. 2, pp. 1079-86.
19. J.S. Kirkaldy, B.A. Thomson, and E. Baganis: *Hardenability Concepts with Applications to Steel*, TMS-AIME, Warrendale, PA, 1978, p. 82.
20. V.G. Rivlin: *Int. Met. Rev.*, 1983, vol. 28, p. 309.
21. V.G. Rivlin and G.V. Raynor: *Int. Met. Rev.*, 1983, vol. 28, p. 23.
22. A. Hultgren: *Jernkontorets Ann.*, 1951, vol. 135, p. 403.
23. M. Hillert: *Jernkontorets Ann.*, 1952, vol. 136, p. 25.
24. E. Rudberg: *Met. Rev.*, 1952, vol. 136, p. 91.
25. J.B. Gilmour, G.R. Purdy, and J.S. Kirkaldy: *Metall. Trans.*, 1972, vol. 3, pp. 1455-65.
26. M. Enomoto and H.I. Aaronson: *Scripta Metall.*, 1985, vol. 19, p. 1.
27. J. Fridberg, L.-E. Torndahl, and M. Hillert: *Jernkontorets Ann.*, 1969, vol. 153, p. 263.